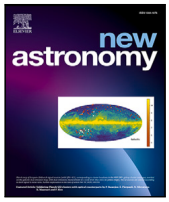
New Astronomy 107 (2024) 102161



Contents lists available at ScienceDirect

New Astronomy

journal homepage: www.elsevier.com/locate/newast



BD UMi: Eccentric detached binary with γ Doradus type component

Birol Gürol

Department of Astronomy and Space Sciences, Ankara University, Science Faculty, Tandoğan, Ankara, 06100, Turkey

ARTICLE INFO

Keywords:
Stars: binaries: eclipsing: pulsation
Stars: fundamental parameters
Technique: photometry
Stars: individual (BD UMi)

ABSTRACT

BD UMi is an Algol-type eccentric eclipsing binary with one of the components showing γ Doradus type pulsation. In this study we used the Transiting Exoplanet Survey Satellite (TESS) observations of the BD UMi system published in total of 16 sectors. We obtained the minima times of the eclipsing system and refined new light elements by using $(O-C)$ technique. Out-of-eclipse variation related to the pulsation was analysed in the frequency domain and g-mode pulsations were detected at frequencies $< 2d^{-1}$. We analysed the light curve of the system and obtained the physical and geometrical parameters of the components by using the well-known Wilson–Devinney code.

We found that the amplitude and frequency of the pulsation are variable and obtained three significant frequency as $f_1 = 0.588d^{-1}$, $f_2 = 0.746d^{-1}$, and $f_3 = 0.140d^{-1}$ which can be used as mean frequencies of the pulsator.

We found that the primary component is a γ Doradus type star. In this work the BD UMi system has been analysed in detail for the first time and we obtained masses and radii of the primary and secondary components as $M_1 = 1.743 \pm 0.011 M_\odot$, $M_2 = 1.734 \pm 0.014 M_\odot$ and $R_1 = 1.937 \pm 0.004 R_\odot$, $R_2 = 1.266 \pm 0.002 R_\odot$, respectively.

1. Introduction

Investigations of pulsating stars in eclipsing binaries give us important restrictions for the improvement of stellar theories because two different ways of measuring the physical properties of stars are possible at the same time. Pulsating variables can be used to investigate the internal structure of stars. Eclipsing binary systems are important objects for understanding the physics of stellar structure and evolution, because they are the only stars whose masses and radii can be measured from observations.

BD UMi (TIC 272650576, HD 139388, $V = 9^m.15$, (B-V)=0.26, $\alpha_{2000} = 15^h32'57''.48$, $\delta_{2000} = +70°42'15''.80$) is classified as a Spectroscopic Binary in the Simbad database and the spectral type and distance of the system are given as A2 (Cannon and Pickering, 1993) and 281 pc (Gaia Collaboration, 2020), respectively. Davies (2015) obtained the first light curve and calculated the light elements of the system and phase of the secondary eclipse as $JD(Min.I) = 2456423.231+16.2570\times E$ and 0.544, respectively. Additionally, the eclipse duration and depth of the primary and secondary minima were given as 4.7 hr with 0.28 mag, 7.8 hr with 0.18 mag, respectively. In the catalogue of galactic eclipsing binary stars with eccentric orbits based on eclipse timing diagrams Kim et al. (2018) gave the systems light elements and phase of the secondary minima as $JD(Min.I) = 2456423.591 + 16.2567200\times E$ and 0.544, respectively which was cited the publication of Davies (2015).

In the "ASAS-SN Catalog of Variable Stars: II", Jayasinghe et al. (2019) lists the following properties for this target: $V = 9^m.13$, Amp=$0^m.52$ with non-periodic "ROT:" variable including the colour excess as $E(B-V) = 0.022$. There is total of 515 observations in V filter which the time span is nearly 1679 days. The data seems to be scattered at the maxima and cannot see any periodic variation related to the pulsation.

Additional photometric observations found in the KWS[1] (Kamogata /Kiso /Kyoto Wide-field Survey) database. Total of 242 observations obtained in V and Ic filter. The time span of observations is nearly 161 days. Since it was observed in a survey, a maximum of 4 points were taken on each observing night.

Since there is no detailed study about the system in the literature and it is understood that the physical parameters of the components can be obtained with the available data found in the catalogues, it is thought that an important contribution to the literature can be made with the solution of the system.

The obtained amplitude and period of the pulsation, together with the temperature of the primary component, shows that the primary

E-mail address: birol.gurol@ankara.edu.tr.

[1] http://kws.cetus-net.org/~maehara/VSdata.py

https://doi.org/10.1016/j.newast.2023.102161
Received 1 September 2023; Received in revised form 1 November 2023; Accepted 15 November 2023
Available online 18 November 2023
1384-1076/© 2023 Elsevier B.V. All rights reserved.

Table 1
The eclipse times of the BD UMi system.

No	Type	BJD (2450000+)	$\pm\sigma$	No	Type	BJD (2450000+)	$\pm\sigma$
1	II	8691.76227	0.00001	25	II	9390.80499	0.00001
2	I	8699.20575	0.00001	26	I	9398.24932	0.00004
3	II	8708.02199	0.00001	27	II	9407.06033	0.00001
4	I	8715.46272	0.00001	28	I	9414.50711	0.00001
5	I	8731.71977	0.00002	29	II	9423.33019	0.00008
6	II	8740.53474	0.00001	30	I	9430.76202	0.00002
7	I	8747.97573	0.00003	31	II	9439.57660	0.00001
8	II	8756.79184	0.00001	32	II	9585.88821	0.00001
9	I	8845.51507	0.00002	33	II	9602.14142	0.00001
10	II	8854.33170	0.00007	34	I	9609.58748	0.00002
11	I	8861.77329	0.00001	35	II	9618.40490	0.00007
12	II	8870.58046	0.00002	36	I	9625.84581	0.00002
13	I	8878.03030	0.00003	37	II	9634.65895	0.00001
14	II	8886.84729	0.00001	38	I	9642.10093	0.00003
15	I	8894.28799	0.00001	39	I	9658.35996	0.00002
16	II	8903.10523	0.00001	40	II	9667.17133	0.00001
17	I	8910.54304	0.00001	41	I	9674.61537	0.00002
18	II	8919.36174	0.00007	42	II	9683.42596	0.00008
19	II	8935.61623	0.00001	43	I	9690.87200	0.00002
20	I	8943.05857	0.00003	44	II	9748.45479	0.00007
21	II	8951.87140	0.00001	45	I	9755.89956	0.00003
22	II	9016.90244	0.00001	46	II	9764.71492	0.00001
23	I	9024.34042	0.00001	47	II	9829.74102	0.00001
24	II	9033.15518	0.00002	48	I	9837.18406	0.00001

component of the eclipsing binary BD UMi is most probably a GDOR type pulsator.

2. The *TESS* data and light elements

The observations of BD UMi were made by the Transiting Exoplanet Survey Satellite (*TESS*) (Ricker et al., 2015) at total of 16 sectors (14, 15, 16, 20, 21, 22, 23, 26, 40, 41, 47, 48, 49, 50, 53, and 56) which each sector has $\sim$ 27.4 days of observations with nearly 2 min (SC: Short Cadence) exposure time. The *TESS* data are public in the MAST (Barbara A. Mikulski Archive for Space Telescopes[2]) archive. In this study we prefer to use the raw SAP (simple aperture photometry) data because of it overlaps with PDCSAP (pre-search data conditioning) data very well and contains more data then PDCSAP data. We have checked the light curve because of the possibility of contamination by a nearby star but do not find any sign of contamination. For this we used different combination of pixel masks around the star and see that all of them show pulsational variation. A total of 294,341 observations of the system were obtained and the time span is nearly 1170 days. The light elements of the system are given in the *TESS* Eclipsing Binary Catalogue (Prša et al., 2022) as,

$$Min.I(BJD) = 2458878.029124(0.000373) + 16.2567430(0.0000183) \times E \quad (1)$$

As can be seen in Fig. 1 the system is a detached binary with different depth of minima. All primary and secondary minima located nearly in the same orbital phases which shows us that the light elements given by Prša et al. (2022) is well defined. Because of the different eclipse duration and secondary minima occurred out of the 0.5 phase the orbit of the system's eccentricity must be larger than zero. Additionally, out of eclipse variation seems to be periodic which can be interpreted as pulsational variation in the system.

Using the observations, we obtained 22 primary and 26 secondary eclipse times. The eclipse times were calculated using the *Minima*27[3] software published by Dr. Bob Nelson. In Table 1 we give the calculated minima times including the errors obtained with the same software.

Using the calculated eclipse times, we obtained the $(O-C)$ variation as given in Fig. 2. Using a linear fit separately on the $(O-C)$ data we obtained new light elements for primary and secondary minima as,

$$Min.I(BJD) = 2458878.03039(0.00024) + 16.256838(0.000074) \times E \quad (2)$$

$$Min.II(BJD) = 2458855.01974(0.00086) + 16.256808(0.000268) \times E \quad (3)$$

The difference in orbital periods obtained for primary and secondary minima is about 2.65 s and it is larger than the error obtained for secondary minima. Essentially in Fig. 2 we see that the slope of the linear fits is different with each other. If it is not caused because of the pulsational variation seen in the secondary minima (see Fig. 5) this can be sign of the possible apsidal motion for BD UMi which can be proven in the future observations. For the rest of calculation, we used the light elements obtained for the primary minima.

3. Light curve analysis

Because of the calculation time we obtained a total of 1000 points by averaging at 0.001 phase intervals by using all of the observations (see Fig. 3). As can be seen in Fig. 3 the normal points obtained by averaging of all observations substantially eliminates the pulsational variation. By using this phase intervals, we see that the depth of both minima was not changed. For the light curve analysis, we prefer to use the Wilson–Devinney (2015 version which in 2019 the *TESS* band added to the code) code which can solve light curves in magnitudes or in flux. The Wilson & Devinney method (Wilson and Devinney, 1971; Wilson, 1979, 1990; Wilson and van Hamme, 2007) was applied to solve the light curve of the BD UMi system.

In Table 2 we compiled effective temperatures published in different sources except the last one which is obtained according to the log $T_{\rm eff} - (B-V)_0$ relation given by Eker et al. (2020) with using the $(B-V) = 0.26$ colour and $E(B-V) = 0.022$ reddening values found in the ASAS-SN catalogue (Jayasinghe et al., 2019). Excluding the most divergent temperature given in Table 2 the median and standard deviation of the effective temperatures were obtained as 7412 ± 108 K and we prefer to use it as primary's temperature in the light curve analysis.

But it must be said that according to the published Spectral type — Temperature tables the temperatures obtained are higher than the median value obtained by using Table 2. Some examples obtained from

[2] https://mast.stsci.edu/portal/Mashup/Clients/Mast/Portal.html
[3] https://www.variablestarssouth.org/resources/bob-nelsons-software-tools/software-by-bob-nelson

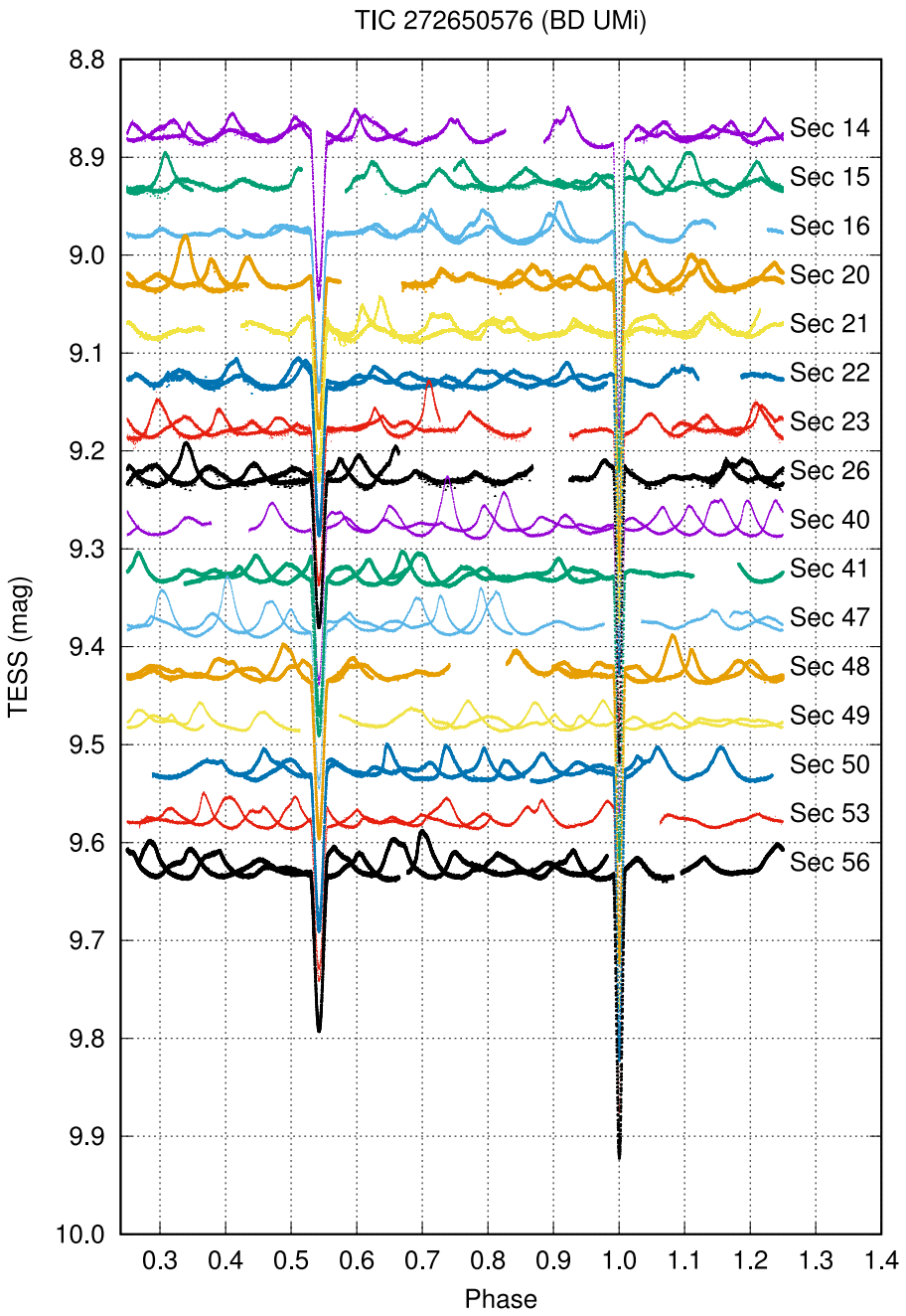


Fig. 1. Light curves of BD UMi obtained by *TESS*. Magnitudes for different sectors are shifted by adding 0.05 mag relatively to the previous sector. Phase values obtained with the light elements given by Prša et al. (2022).

Table 2
$T_{\rm eff}$ values obtained from different sources for BD UMi.

$T_{\rm eff}(K)$	References
8970	Wright et al. (2003)
7481	Stassun et al. (2019)
7590	Ammons et al. (2006)
7452	*Gaia* DR2, Gaia Collaboration (2018)
7301	*Gaia* DR3, Gaia Collaboration (2022)
7452	Tonry et al. (2018)
7220	Stevens et al. (2017)
7273	McDonald et al. (2017)
7315	Bai et al. (2019)
7481	Prša et al. (2022)
7553	$\log T_{\rm eff} - (B-V)_0$ relation, Eker et al. (2020)

literature are 9000 K (Cox, 1999), 9078 K (Eker et al., 2020), 9730 K (Zombeck, 2004), 8900 K (Gray et al., 2008), 9141 K (Straizys and Kurilliene, 1981). Including the excluded temperature from Table 2, the median of these values is 9039 ± 303 K which is nearly 1627 K higher than the temperature accepted for light curve solution. Gebran et al. (2023) compared some of the stellar parameters of AFGK stars including $T_{\rm eff}(K)$ values published in the Vizier catalogue with the parameters obtained by spectral data and showed that large discrepancies can be found in the effective temperature of the stars. The large discrepancy probably caused because of quality of data (spectra and/or photometric) and different analysis methods.

Before light curve analysis we can find eccentricity and argument of periastron of the orbit by using the widths of the primary (ω_1) and secondary (ω_2) eclipses and the phase of the secondary eclipse (φ_2). The required data given as 0.015, 0.021, and 0.542, respectively by Prša

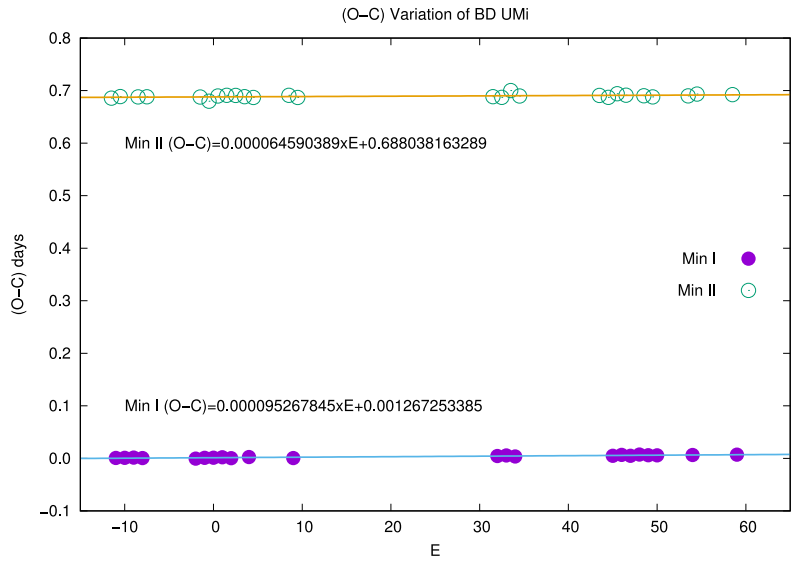


Fig. 2. The $(O-C)$ variation of the BD UMi system.

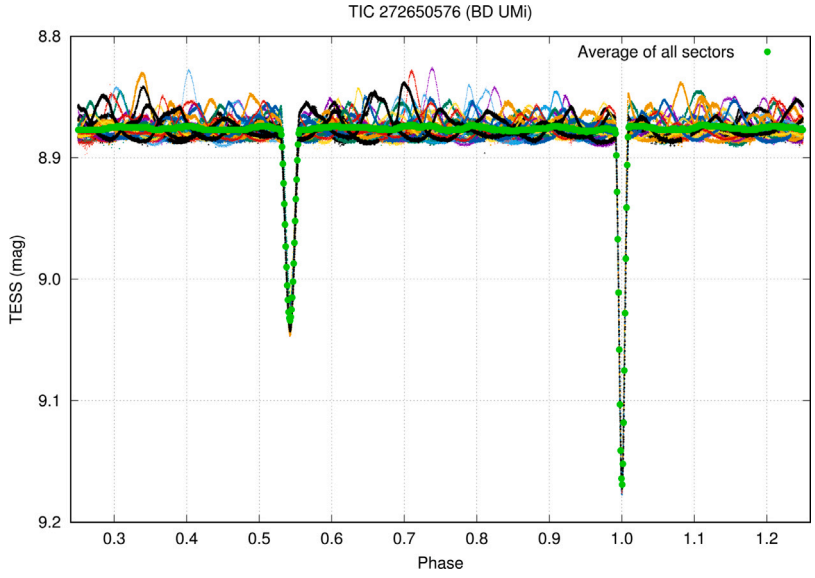


Fig. 3. The constructed light curves of BD UMi for all sectors and normal points obtained by averaging observations over a phase interval of 0.001.

et al. (2022). Using the formulae given by Kopal (1978) (Eqs. (4) and (5)) and the phase of the primary eclipse as $\varphi_1 = 0$ we obtained the eccentricity and argument of periastron as 0.2044 and 71.01 deg, respectively. And it is used as input parameters in the light curve analysis of the eclipsing system.

$$e_0 cos\omega_0 = \frac{\pi}{2}\left[(\varphi_2 - \varphi_1) - 0.5\right] = 0.0665 \tag{4}$$

$$e_0 sin\omega_0 = \frac{\omega_2 - \omega_1}{\omega_2 + \omega_1} = 0.1933 \tag{5}$$

In the catalogue of *Gaia* DR3 Part 3 for non-single stars (Gaia Collaboration, 2022) we found the systems velocity of centre of mass as $V_\gamma = -2.128 \pm 0.253$ km/s, semi-amplitude of the primary and secondary component as $K_1 = 66.878 \pm 0.508$ km/s and $K_2 = 66.543 \pm 0.473$ km/s, respectively. Additionally, the system's eccentricity $e = 0.089 \pm 0.006$ and the argument of periastron $\omega = 321.601 \pm 4.507$ deg were obtained which are not compatible with the calculated data by using Eqs. (4) and (5). The worst thing is that the orbital period given in the catalogue is 4.649853 ± 0.000057 days which is nearly 11.6 days shorter, or nearly 3.5 times smaller than the real orbital period. If it is possible the *Gaia* DR3 data should be reanalyzed for verify the orbital period of this system. According to the given values in *Gaia* DR3 catalogue the mass ratio of the system is obtained as $q(m_2/m_1) = 0.995$.

The distance of the closest star (d = 4.465 arcmin) with nearly same magnitude is HD 139476 which the spectral type is given as G5 in the Simbad database. Therefore, we think that misidentification with BD UMi is not possible. Because of the amplitudes of the radial velocity data published in *Gaia* DR3 cannot change with taking different orbital period we think that it can be used in the light curve analysis for obtaining absolute parameters of the components.

In the light curve analysis of the BD UMi system, we used Mode 2 for appropriate Algol type systems. Additionally, we select the starting parameters as $T_{eff,1}(K) = 7412$, $e = 0.2044$, $\omega(deg) = 71.01$, P(day) = 16.25683827. Because of the temperature of the primary component is higher than 7200 K we used the primaries albedo and gravity darkening parameters as 1.0. And because of we assumed the secondary temperature is lower than the primary's we select $T_{\rm eff}(K) = 7000$ including albedo and gravity darkening parameters as respectively, 0.5 and 0.32.

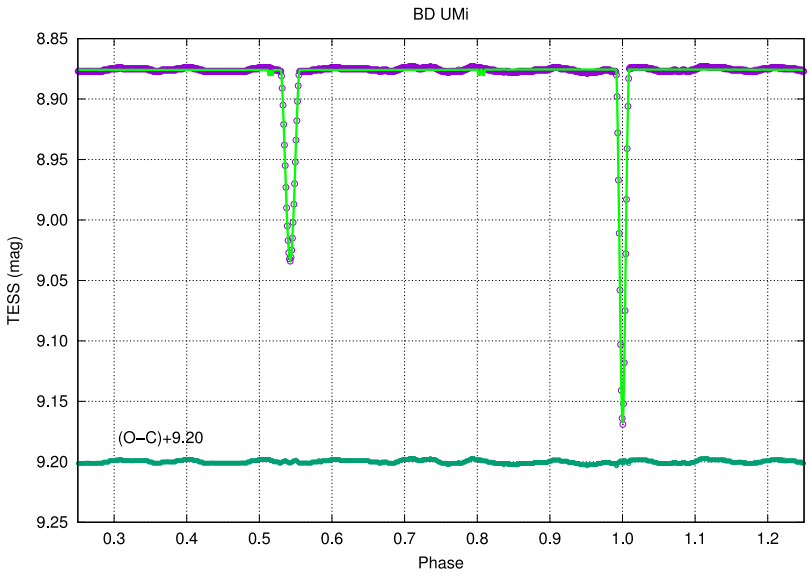


Fig. 4. The observational and theoretical light curves of BD UMi including the residuals of the fit.

By using the initial parameters (T_1, q, i, e, ω) as input values we solved the light curves until the solution converged. The convergent solution was obtained with the adjustable parameters by iteration, until the correction on the parameters became smaller than the corresponding standard deviations. We see that the convergent solution was obtained when the temperature of the secondary component goes to higher values. Because of this we adjust again the albedo and gravity darkening values as 1.0 and iterate the solution until the best fit obtained with the observations.

The observed and theoretical light curves, calculated with the final elements, are shown in Fig. 4 including the residuals of the fit with the observations. The parameters obtained from the light curve analysis are given in Table 3.

The absolute parameters of the components obtained by the Wilson–Devinney LC code for the BD UMi system are given in Table 4. Because the LC code does not produce any error for the absolute parameters, we estimated them from the input parameters. Since the light curve solution give very small error for the secondary' temperature (like ±14 K), we accepted the error as ±100 K. The errors given here correspond to the propagated errors of the calculated parameters.

By using the semi-major axis and the mean fractional radii obtained by the light and radial velocity solution, we can find the radii of the components in solar unit separately. The mean fractional radii of components were calculated with the formula, $r_{\rm mean} = (r_{\rm pole} \times r_{\rm side} \times r_{\rm back})^{1/3}$ as 0.04734 ± 0.00007 and 0.03092 ± 0.00005 for primary and secondary components, respectively. Using those values we can calculate the radii of the components as $R_1 = a \times r_{1,\rm mean} = (1.937 \pm 0.004)\mathrm{R}_\odot$ and $R_2 = a \times r_{2,\rm mean} = (1.266 \pm 0.002)\mathrm{R}_\odot$.

The absolute parameters of $M_{\rm bol1,2}$ and $L_{1,2}$ can be calculated using the well-known equations (6) and (7) respectively,

$$M_{\rm bol1,2} = 4^m.74 - 5log(R_{1,2}/\mathrm{R}_\odot) - 10log(T_{1,2}/\mathrm{T}_\odot) \quad (6)$$

$$L_{1,2}(L_\odot) = (R_{1,2}/\mathrm{R}_\odot)^2 (T_{1,2}/\mathrm{T}_\odot)^4 \quad (7)$$

Adopting $T_\odot = 5772\,\mathrm{K}$, the bolometric magnitudes are found to be $M_{\rm bol1} = 2.128 \pm 0.063$ and $M_{\rm bol2} = 2.909 \pm 0.056$, and luminosities $L_1 = (10.205 \pm 0.596)\mathrm{L}_\odot$ and $L_2 = (5.452 \pm 0.279)\mathrm{L}_\odot$ for the primary and secondary component, respectively.

Using the $BC_{TESS} - T_{\rm eff}$ relation given for main sequence stars by Eker and Bakış (2023) we obtained bolometric correction for the primary and secondary component as 0.21 ± 0.07 and 0.12 ± 0.07, respectively. Since the bolometric magnitude of the components are known we can calculate the absolute magnitude of the components separately using the formula $M_{TESS} = M_{\rm bol} - BC_{TESS}$ which we obtained $M_{TESS,\rm pri} = 2^m.017 \pm 0.094$ and $M_{TESS,\rm sec} = 2^m.787 \pm 0.089$, respectively. Using the system's magnitude as $TESS = 8^m.878 \pm 0.004$ and light ratios obtained from the solution as $L_1/L_2(TESS) = 2.02519 \pm 0.00027$, we can obtain the magnitude of the primary and secondary component as $T_{pri.} = 9.314 \pm 0.008$ and $T_{sec.} = 10.078 \pm 0.013$, respectively. Because the interstellar extinction in TESS filter can be obtained with the relation given by Stassun et al. (2019) as $A(TESS) = 2.06 \times E(B-V) = 0^m.04532$, we can calculate the distance of the primary and secondary component respectively as,

$$d_1(pc) = 10^{[(T_{pri.} - A(T) - M_{TESS,pri.} + 5)/5]} = 282.07 \pm 5.35 \quad (8)$$

$$d_2(pc) = 10^{[(T_{sec.} - A(T) - M_{TESS,sec.} + 5)/5]} = 281.30 \pm 5.08 \quad (9)$$

Table 3
The light curve solution of BD UMi using *TESS* observations. The assumed values are marked with * symbol.

Parameter	Solution	±σ
T_0 (BJD)	2458878.03039	0.000242
P (day)	16.25683827	0.0000738
a ($\mathrm{R}_\odot$)	40.927	–
V_γ (km/s)	−2.128*	0.253*
K_1 (km/s)	66.878*	0.508*
K_2 (km/s)	66.543*	0.473*
$q(m_2/m_1)$	0.995*	0.005*
Phase Shift	0.0171	–
e	0.271	0.001
ω (deg)	76.326	0.028
i (deg)	87.786	0.006
T_1 (K)	7412*	108*
T_2 (K)	7840	100*
A_1	1.0	–
A_2	1.0	–
g_1	1.0	–
g_2	1.0	–
Ω_1	22.49148	0.05456
Ω_2	33.55196	0.08534
x_1(bolo)	0.644	–
x_2(bolo)	0.638	–
y_1(bolo)	0.263	–
y_2(bolo)	0.254	–
$L_1/L_{tot.}$ (*TESS*)	0.66901	0.00270
r_1(mean)	0.04734	0.00007
r_2(mean)	0.03092	0.00005
σ(fit)	–	8.37924E−8

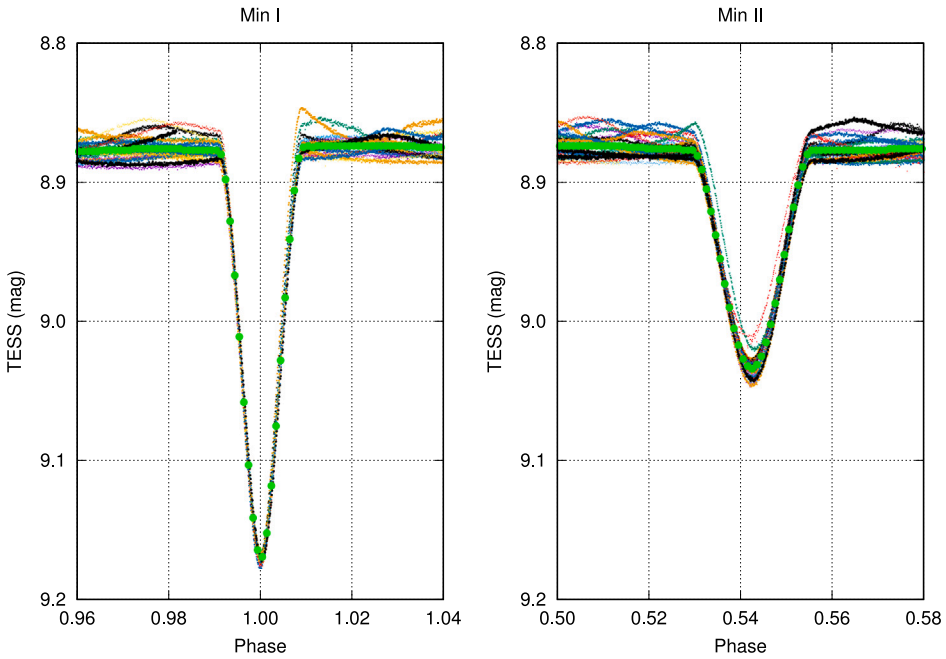


Fig. 5. The constructed light curves of BD UMi around primary and secondary minima for all sectors and normal points plotted as green dots.

Table 4
Absolute parameters of BD UMi.

Parameters	Primary	Secondary
Mass ($M_\odot$)	1.743 ± 0.011	1.734 ± 0.014
Radius ($R_\odot$)	1.937 ± 0.004	1.266 ± 0.002
Luminosity* ($L_\odot$)	10.205 ± 0.596	5.452 ± 0.279
$\rho(\rho_\odot)$	0.240	0.856
M_{bol}	2.228 ± 0.063	2.909 ± 0.056
Bol.Corr.(TESS)	0.21 ± 0.07	0.12 ± 0.07
M_{TESS}	2.017 ± 0.094	2.787 ± 0.089
log g (cgs)	4.105 ± 0.003	4.473 ± 0.004
d(pc)	282 ± 5	281 ± 5

* Calculated by using components' temperature and radius.

The distance to the system evaluated from light curve solution is consistent with that given in the *Gaia* DR3 Part 1 (Gaia Collaboration, 2022) and *TESS* (Stassun et al., 2019) catalogues as 277.6 pc and 278.999 pc, respectively. This compatibility can be considered as a support of the reliability of the light curve solution.

4. Pulsational analysis

In Fig. 5 we plotted the light curves around primary and secondary minima to see the effect of pulsation in the eclipse. As can be seen at the primary minima we do not see any pulsational variation but at the secondary minima it can be seen. According this we can say that the primary component is the pulsator in the system. However, if the pulsation cancelled and/or affected due to the proximity effect, as the components are closest to each other due to orbital eccentricity there is a possibility of the secondary component can be the pulsator too.

To investigate the nature of the pulsation we prefer to extract the minima from the observations and use those clipped data to get information about the pulsation as done by Debosscher et al. (2013), Maceroni et al. (2013, 2014, 2015), Li et al. (2020), and Gürol (2023).

In order to reveal the nature of the pulsation we prefer to use the Fourier analysis package Period04 (Lenz and Breger, 2005) which performs analysis in the frequency domain. Because of the large data we prefer to obtain the amplitude spectrum for sectors separately. The amplitude spectrum obtained for the out-of-eclipse variation is given in Fig. 6 and the obtained results are given in Table A.5 including the frequency, period, amplitude, phase values and combination of frequencies following the method described in Zhang et al. (2019, 2020) in the form of $f_i = mf_j \pm nf_k$ where m and n are integers less than 3 (Kurtz et al., 2015). The mean Rayleigh resolution obtained for all sectors is found to be $1/\Delta T = 1/26.62117d = 0.00375d^{-1}$. All of the marked combinations given in Table A.5 are obtained as the difference between the observed and predicted frequency are lower than the Rayleigh criterion.

We see that some of the obtained frequencies are found to be harmonics of the previous ones. Relatively few of the frequencies are related to the orbital frequency ($f_{orb} = 0.061512576d^{-1}$) in the form of $f_i \pm kf_{orb}$ ($k = 1,2,3, \ldots$).

It seems that both frequency and amplitude are changing (see Fig. 6) which can be explained with superposition of several base frequencies with changing phases. All of the frequencies are located at the period range $0.47 < P(day) < 41.18$ ($0.024 < f(d^{-1}) < 2.11$). The maximum amplitude reached at 0.01 mag in Sector 56. In Fig. 7 we plotted the period distribution obtained by Fourier analysis and see that most of the periods are smaller than 3 days.

In Fig. 8 we plotted amplitude–frequency distribution obtained by frequency analysis. As can be seen in the figure the frequencies seems to be clustered at four different region. We prefer to fit a Bezier curve to all of the data given in Table A.5 by using $GNUPLOT v5.4$[4] and mark the peaks visually. The obtained frequencies are $f_1 = 0.588$ ($P_1 = 1.70068$ day), $f_2 = 0.746$ ($P_2 = 1.340483$ day), $f_3 = 0.140$ ($P_3 = 7.142857$ day), and $f_4 = f_1 + f_2 = 1.334$. Probably the f_4 frequency is the harmonics of the f_1 and f_2. The frequencies obtained by this way can be used as mean pulsational frequencies for BD UMi system.

The binary model yields a mean density of $\rho_1 = 0.240\rho_\odot$ and $\rho_2 = 0.856\rho_\odot$ for primary and secondary component, respectively. Using the mean f_1 frequency and the relation ($Q = P_{\rm puls}\sqrt{\rho/\rho_\odot}$) given for pulsation constant we obtained pulsation constants as $Q_1 = 0.833$ and $Q_2 = 1.573$ days for the primary and secondary component, respectively.

Kaye et al. (1999) characterized the γ Doradus (GDOR) type variables as high-order, low-degree, non-radial gravity mode pulsators and showed that the period range is $0.3 \leq P(day) \leq 3$ ($0.33 \leq f(d^{-1}) \leq 3.33$).

[4] http://www.gnuplot.info/

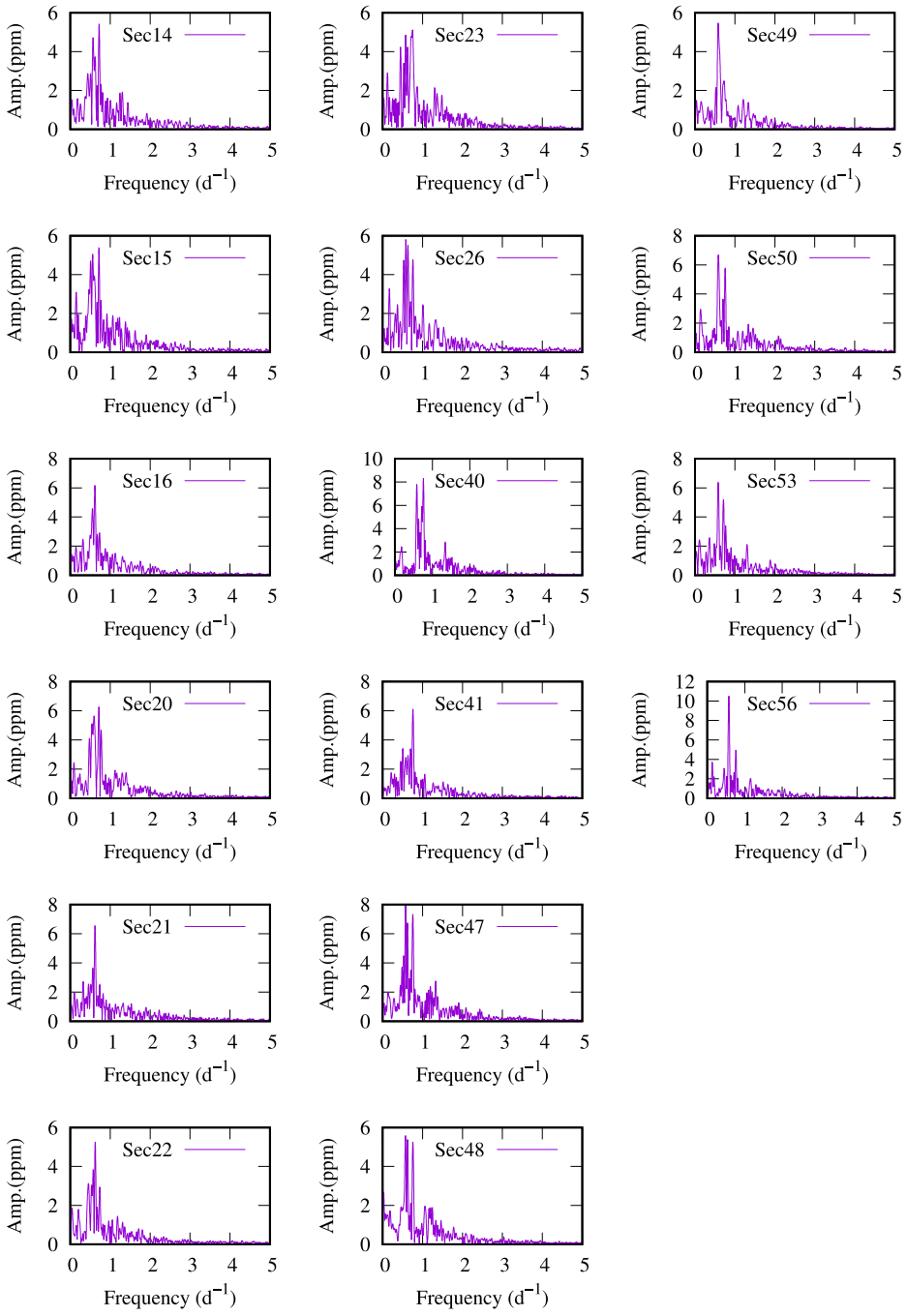


Fig. 6. The amplitude spectrum for the out-of-eclipse light variation of BD UMi for different sectors.

Among the GDOR type pulsators there are low- and high-amplitude examples which the high-amplitude ones explained by the superposition of several base frequencies (Paunzen et al., 2020). Most of the GDOR pulsators are in the region of A and F-type main sequence stars which the temperature range of $6100 < T_{eff} < 7500$ K (Bradley et al. 2015). Additionally, Q pulsation constants for GDOR type stars is given as $Q > 0.24$ days (Grigahcène et al., 2010).

All of the parameters obtained for the primary component; effective temperature ($T_1 = 7412$ K), Q pulsation constant ($Q_1 = 0.833$ days), and frequency of the periodic variation ($f = 0.588 d^{-1}$) shows us that the primary component can be a GDOR type pulsator. In Fig. 9 we see that the primary component is located out of the instability strip given for GDOR type pulsators. But we also see that a small number of GDORs are located outside this instability strip too which can be a sign of confirmation of the type of the pulsator.

5. Result and discussions

We derived for the first time the absolute and geometrical parameters of the Algol type eccentric eclipsing binary BD UMi by using *TESS* and *Gaia* observations. The results of light-curve modelling reveal that BD UMi is a detached system. Using the semi-amplitudes of the radial velocity data of the system given in the catalogues with our light curve solution enabled us to find the physical and geometric parameters of the components. In this sense, we conclude that the system will make an important contribution to the literature.

We updated the light elements of the system by using all of the times of minima obtained by the *TESS* observations. The difference of the orbital period obtained for primary and secondary minima is nearly 2.6 s and it is larger than the error obtained for secondary minima.

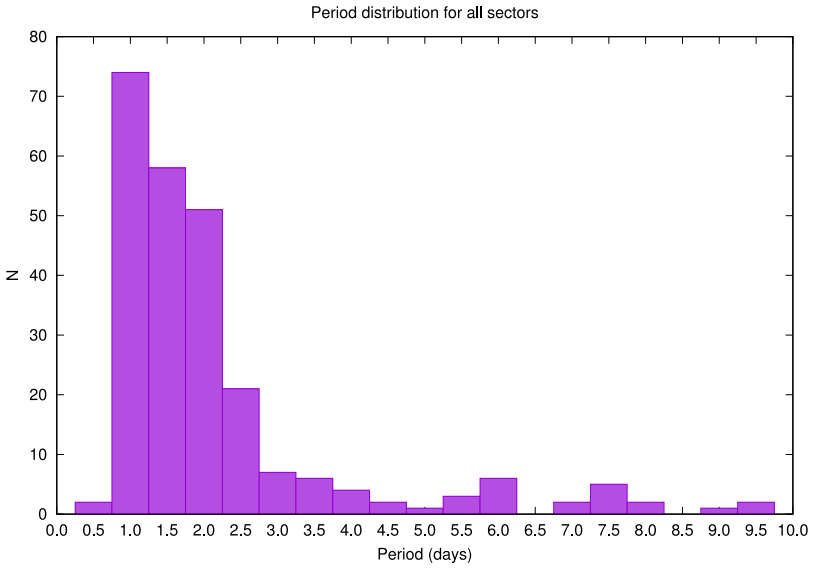


Fig. 7. Period distribution obtained from data given in Table A.5. The periods larger than 10 days were excluded.

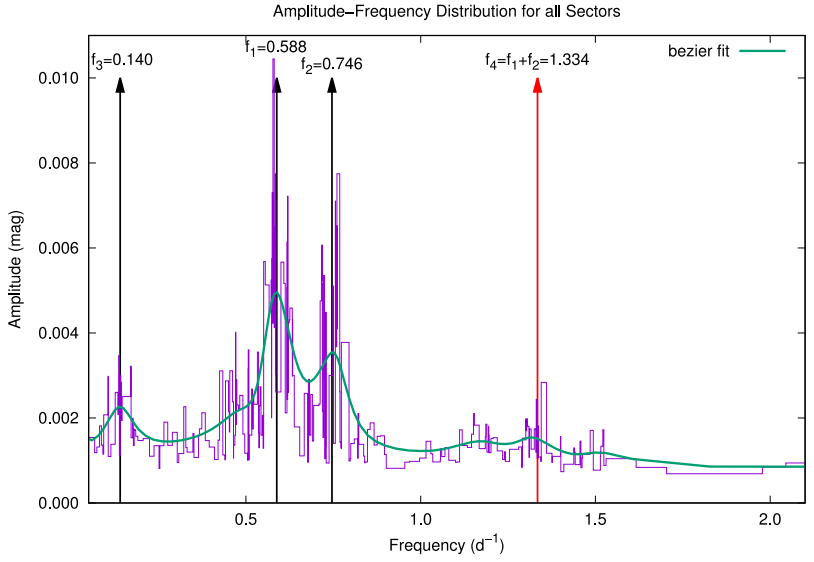


Fig. 8. Amplitude-Frequency distribution of all sectors obtained from Table A.5 including Bezier curve fit.

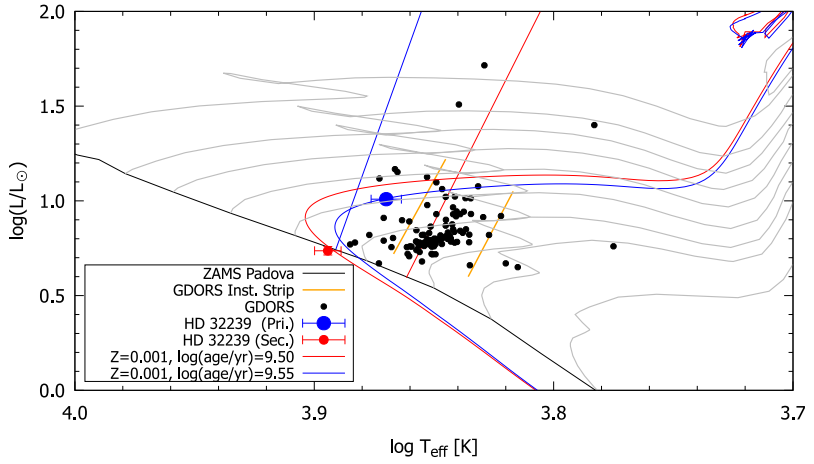


Fig. 9. Position of the primary and secondary component of BD UMi on Hertzsprung–Russell diagram (blue and red points respectively). Black dots show confirmed γ Doradus stars compiled from Kaye et al. (1999), Henry et al. (2005), and Paunzen et al. (2020). Dotted blue and red lines represent the boundaries of the instability strip (blue and red edges). Orange lines indicate theoretical cool and hot boundary of γ Doradus instability strip (Warner et al., 2003). Black line show ZAMS and grey dashed lines show evolutionary tracks of stars with varying mass for solar metallicity composition Z = 0.008 were taken from Girardi et al. (2000). Blue and red solid lines shows isochrones obtained from PARSEC for Z = 0.001 (Chen et al., 2015).

Additionally, we find sign of possible apsidal motion for BD UMi which can be proven in the future observations.

We found that the amplitude and frequency of the pulsation are variable. And obtained three significant frequency as $f_1 = 0.588d^{-1}$, $f_2 = 0.746d^{-1}$, and $f_3 = 0.140d^{-1}$ which can be used as mean frequencies of the pulsator.

In Fig. 9 we plot our results with the GDOR type variables compiled from Kaye et al. (1999), Henry et al. (2005), and Paunzen et al. (2020). The primary component is located in the instability strip where a bit away from the hot boundary of γ Doradus instability strip. But as can be seen there are other samples which located in the same region. According to the findings we conclude that the primary component in this system is very likely a GDOR type variable. Additionally, we found that the secondary component located on the ZAMS and is hotter than the primary component with lower luminosity.

Using the [Fe/H] value of −0.4375 provided in the Gaia catalogue, we determined the system's metallicity to be Z = 0.005, indicating that the system is composed of metal-poor stars. Initially, we compared the system's location in the HRD with precalculated isochrones from the PARSEC database (Chen et al., 2015) for Z = 0.004, but we could not find a reliable solution for this attempt. After several trials, we found that isochrones with Z = 0.001 are a better fit for the components of BD UMi. Using the fitted isochrones, we estimated the age of the system to be log(age/yr) = 9.50-9.55, corresponding to 3.16–3.55 Gyr.

CRediT authorship contribution statement

Birol Gürol: Formal analysis, Investigation, Data curation, Writing – original draft, Review & editing, Visualization.

Declaration of competing interest

The authors have no conflict of interest to declare.

Data availability

Data will be made available on request.

Acknowledgments

We thank the anonymous referees for helpful comments and suggestions that improved the quality of this paper. This research has made use of VizieR the Simbad database, operated at CDS, Strasbourg, France, and NASA's Astrophysics Data System Abstract Service. This work has made use of data from the European Space Agency (ESA) mission *Gaia* (https://www.cosmos.esa.int/gaia), processed by the *Gaia* Data Processing and Analysis Consortium (DPAC[5]). Funding for the DPAC has been provided by national institutions, in particular the institutions participating in the *Gaia* Multilateral Agreement. The *TESS* data presented in this paper were obtained from the Mikulski Archive for Space Telescopes (MAST). Funding for the *TESS* mission is provided by the NASA Explorer Program. All of the figures were generated by using a freeware software GNUPLOT.

Appendix. The obtained significant frequencies of BD UMi using out of eclipse data

Table A.5 displays the significant frequencies, period, amplitude and phase values of the Fourier analysis and possible linear combinations.

[5] https://www.cosmos.esa.int/web/gaia/dpac/consortium

Table A.5
The obtained significant frequencies of BD UMi using out of eclipse data.

No	Frequency (d^{-1})	Period (days)	Amplitude (mag)	Phase (rad)	Combination
Sector 14					
1	0.72254	1.38401	0.00535	0.44699	...
2	0.57356	1.74349	0.00574	0.35316	...
3	0.62198	1.60777	0.00425	0.59468	...
4	0.42458	2.35525	0.00311	0.79667	$2f_2 - f_1$
5	0.48231	2.07334	0.00253	0.79592	...
6	1.30355	0.76714	0.00198	0.45551	$f_{13} + f_{orb}$
7	0.81006	1.23447	0.00151	0.68657	$f_{10} - f_5$
8	0.03724	26.84980	0.00160	0.85701	...
9	0.36686	2.72587	0.00174	0.70371	$2f_4 - f_5$
10	0.88455	1.13052	0.00158	0.23708	...
11	1.43949	0.69469	0.00120	0.99179	...
12	0.76909	1.30023	0.00144	0.91949	...
13	1.24209	0.80509	0.00098	0.25587	$f_6 - f_{orb}$
14	1.10429	0.90556	0.00097	0.86513	$f_3 + f_5$
15	0.83986	1.19068	0.00094	0.82963	...
16	0.25140	3.97775	0.00081	0.03737	$2f_9 - f_5$
Sector 15					
1	0.71800	1.39276	0.00516	0.50255	...
2	0.56634	1.76573	0.00450	0.75962	$f_9 - 3f_{orb}$
3	0.60857	1.64319	0.00517	0.81240	...
4	0.47035	2.12608	0.00402	0.47806	...
5	0.50682	1.97307	0.00360	0.32796	...
6	0.14590	6.85382	0.00250	0.16506	...
7	0.02880	34.72605	0.00300	0.71596	...
8	1.18643	0.84287	0.00185	0.37835	...
9	0.75064	1.33220	0.00140	0.93964	$f_2 + 3f_{orb}$
10	0.18238	5.48306	0.00171	0.34043	...
11	1.28050	0.78095	0.00132	0.86749	...
12	0.06719	14.88259	0.00118	0.42058	$f_{15} - f_4$
13	1.37649	0.72649	0.00110	0.90398	...
14	0.43387	2.30483	0.00113	0.10461	$2f_4 - f_5$
15	0.53754	1.86032	0.00130	0.97587	$f_2 - f_7$
16	1.23442	0.81009	0.00102	0.86875	$2f_1 - 3f_{12}$

(*continued on next page*)

Table A.5 (*continued*).

No	Frequency (d^{-1})	Period (days)	Amplitude (mag)	Phase (rad)	Combination
Sector 16					
1	0.61824	1.61751	0.00615	0.36352	...
2	0.55540	1.80051	0.00513	0.67762	...
3	0.50675	1.97336	0.00352	0.88199	$f_7 + 3f_{orb}$
4	0.73783	1.35533	0.00263	0.77240	...
5	0.85539	1.16905	0.00188	0.30916	...
6	0.03041	32.88932	0.00199	0.77803	...
7	0.32229	3.10277	0.00227	0.77178	$f_3 - 3f_{orb}$
8	1.31147	0.76250	0.00174	0.33095	...
9	0.82296	1.21512	0.00138	0.31153	...
10	0.08108	12.33350	0.00181	0.70811	...
11	1.19593	0.83617	0.00118	0.73452	...
12	1.51417	0.66043	0.00109	0.44063	...
13	1.06012	0.94329	0.00109	0.57228	$f_4 + f_7$
14	0.39527	2.52995	0.00132	0.95222	$2f_3 - f_1$
15	1.34390	0.74410	0.00098	0.76989	$3f_2 - f_7$
Sector 20					
1	0.71623	1.39620	0.00523	0.66209	...
2	0.60034	1.66572	0.00567	0.89449	...
3	0.55094	1.81507	0.00568	0.86944	...
4	0.77322	1.29329	0.00378	0.55005	...
5	0.47305	2.11393	0.00290	0.80494	...
6	0.63834	1.56657	0.00179	0.98357	...
7	0.82072	1.21845	0.00211	0.72931	...
8	0.09309	10.74222	0.00207	0.96217	...
9	0.52245	1.91407	0.00232	0.86266	...
10	1.30137	0.76842	0.00170	0.69434	...
11	1.11139	0.89978	0.00172	0.13221	$3f_3 - 3f_{12}$
12	0.18048	5.54073	0.00173	0.92763	...
13	1.40016	0.71420	0.00156	0.76888	...
14	1.14558	0.87292	0.00162	0.00169	...
15	0.68203	1.46621	0.00160	0.30630	...
16	1.43815	0.69534	0.00125	0.54339	...
17	1.36026	0.73515	0.00117	0.01221	$3f_7 - 2f_3$
18	0.22418	4.46075	0.00110	0.02914	$2f_9 - f7$
Sector 21					
1	0.61960	1.61395	0.00722	0.92072	...
2	0.67896	1.47284	0.00291	0.57416	...
3	0.52128	1.91836	0.00250	0.22011	...
4	0.10574	9.45716	0.00298	0.79064	...
5	0.46192	2.16489	0.00238	0.93333	...
6	0.26528	3.76964	0.00190	0.28910	...
7	0.57322	1.74452	0.00200	0.61186	$f_2 - f_4$
8	0.72534	1.37866	0.00104	0.85515	$f_1 + f_4$
9	0.17809	5.61519	0.00135	0.52715	$3f_2 - 3f_1$
10	1.19468	0.83705	0.00160	0.32192	$f_{12} + f_{orb}$
11	0.38400	2.60414	0.00147	0.82075	...
12	1.13346	0.88226	0.00131	0.21394	$f_{10} - f_{orb}$
13	0.30794	3.24734	0.00117	0.37504	$f_7 - f_6$
14	1.30969	0.76354	0.00107	0.28808	...
15	1.53045	0.65340	0.00104	0.40419	$2f_7 + f_{11}$
16	0.77172	1.29581	0.00130	0.13173	...
17	1.46181	0.68408	0.00106	0.14634	...
18	0.84035	1.18997	0.00096	0.43681	...
19	0.03339	29.94766	0.00105	0.30295	$2f_4 - f_9$
Sector 22					
1	0.62564	1.59835	0.00459	0.20796	$f_2 + 3f_{orb}$
2	0.44163	2.26434	0.00287	0.71566	...
3	0.54100	1.84844	0.00274	0.33460	...
4	0.73789	1.35521	0.00300	0.03873	...
5	0.58516	1.70893	0.00261	0.33478	...
6	0.47107	2.12281	0.00185	0.00627	...
7	0.20609	4.85215	0.00152	0.69123	...
8	0.04968	20.12743	0.00154	0.34527	...
9	1.18504	0.84385	0.00156	0.75118	...
10	0.13801	7.24587	0.00113	0.49426	...
11	0.69005	1.44917	0.00146	0.81587	$f_3 + 3f_8$
12	0.96791	1.03316	0.00098	0.00762	$2f_{11} - 2f_7$
13	1.05623	0.94676	0.00102	0.60978	$f_5 + f_6$
14	0.79494	1.25796	0.00099	0.84644	$3f_1 - 2f_3$

(*continued on next page*)

Table A.5 (*continued*).

No	Frequency (d^{-1})	Period (days)	Amplitude (mag)	Phase (rad)	Combination
Sector 23					
1	0.74900	1.33511	0.00510	0.20683	...
2	0.71725	1.39422	0.00607	0.67876	...
3	0.57716	1.73262	0.00423	0.44161	$f_4 + 2f_{orb}$
4	0.45388	2.20321	0.00311	0.03965	$f_3 - 2f_{orb}$
5	0.61825	1.61746	0.00244	0.42557	...
6	0.12701	7.87323	0.00260	0.47905	$f_{10} + 4f_{orb}$
7	0.53607	1.86543	0.00165	0.76080	$2f_3 - f_5$
8	1.30562	0.76592	0.00181	0.93617	...
9	0.66682	1.49966	0.00258	0.80112	...
10	0.28951	3.45406	0.00166	0.76105	$f_7 - 4f_{orb}$
11	1.48493	0.67343	0.00171	0.11682	$f_3 + 2f_4$
12	0.86667	1.15384	0.00136	0.55329	$f_3 + f_{10}$
13	1.11883	0.89379	0.00135	0.79857	...
14	0.02428	41.18306	0.00114	0.81798	...
15	1.18981	0.84047	0.00120	0.00010	...
16	1.02918	0.97165	0.00116	0.79977	$3f_7 - 2f_{10}$
17	1.33737	0.74774	0.00108	0.43895	$3f_4 - f_{14}$
Sector 26					
1	0.58111	1.72084	0.00413	0.81367	...
2	0.75806	1.31916	0.00368	0.53251	...
3	0.63339	1.57881	0.00430	0.90675	...
4	0.53285	1.87669	0.00355	0.49344	$f_{16} + 2f_{orb}$
5	0.17091	5.85087	0.00322	0.18744	...
6	0.37400	2.67378	0.00212	0.01153	$f_{15} - 2f_{orb}$
7	0.68567	1.45843	0.00255	0.49087	$2f_3 - f_1$
8	1.32509	0.75466	0.00174	0.11400	...
9	0.45242	2.21033	0.00167	0.83296	...
10	0.33178	3.01408	0.00120	0.04756	$3f_4 - 2f_3$
11	1.01544	0.98480	0.00145	0.24581	$3f_1 - f_{11}$
12	0.72790	1.37382	0.00134	0.53108	...
13	0.23727	4.21461	0.00135	0.48777	...
14	1.09989	0.90918	0.00096	0.24585	$f_2 + 2f_5$
15	0.49666	2.01346	0.00117	0.83125	$f_6 + 2f_{orb}$
16	0.41020	2.43786	0.00102	0.50409	$f_4 - 2f_{orb}$
17	0.82039	1.21893	0.00105	0.06577	$2f_1 - 2f_5$
18	1.40954	0.70945	0.00091	0.08943	...
19	1.52416	0.65610	0.00088	0.32262	$3f_7 - f_4$
Sector 40					
1	0.76057	1.31480	0.00775	0.07356	...
2	0.58437	1.71126	0.00774	0.00990	...
3	0.72821	1.37323	0.00449	0.08924	$f_{10} + 3f_{orb}$
4	1.34494	0.74353	0.00284	0.34265	$f_1 + f_2$
5	0.62033	1.61205	0.00260	0.71306	...
6	0.17621	5.67509	0.00199	0.85717	$f_1 - f_2$
7	0.14384	6.95198	0.00194	0.95886	$f_3 - f_2$
8	1.52115	0.65740	0.00172	0.42970	$2f_4 - 2f_2$
9	0.80013	1.24979	0.00140	0.79443	...
10	0.54301	1.84158	0.00160	0.95232	$f_3 - 3f_{orb}$
11	0.87565	1.14201	0.00157	0.13681	...
12	0.68506	1.45973	0.00160	0.80358	...
13	1.43844	0.69520	0.00130	0.56370	$2f_6 - 2f_{10}$
14	1.21908	0.82029	0.00123	0.18412	...
15	1.31617	0.75978	0.00127	0.16678	...
16	0.10608	9.42641	0.00109	0.36090	...
17	2.10911	0.47413	0.00085	0.46866	...
18	1.97785	0.50560	0.00084	0.62580	...
19	1.61645	0.61864	0.00084	0.69087	...
Sector 41					
1	0.75972	1.31628	0.00653	0.88402	...
2	0.63373	1.57797	0.00300	0.51585	...
3	0.50585	1.97686	0.00315	0.28117	...
4	0.58483	1.70989	0.00302	0.46918	...
5	0.69390	1.44113	0.00230	0.51765	...
6	0.25387	3.93908	0.00135	0.47984	$f_1 - f_3$
7	1.05684	0.94622	0.00128	0.27462	$2f_6 + f_9$
8	1.51568	0.65977	0.00133	0.89465	...
9	0.54910	1.82115	0.00129	0.66736	...
10	0.08650	11.56033	0.00136	0.90902	...
11	1.25429	0.79726	0.00126	0.07337	...
12	0.46448	2.15294	0.00106	0.71113	$2f_9 - f_2$
13	0.83682	1.19500	0.00110	0.70841	...

(*continued on next page*)

Table A.5 (*continued*).

No	Frequency (d^{-1})	Period (days)	Amplitude (mag)	Phase (rad)	Combination
14	1.44234	0.69332	0.00090	0.08445	$3f_1 - f_{13}$
15	0.72963	1.37055	0.00094	0.64416	...
16	1.40097	0.71379	0.00074	0.66012	...
17	1.70373	0.58695	0.00069	0.44519	$2f_{16} - 2f_9$
Sector 47					
1	0.57511	1.73880	0.00730	0.88665	...
2	0.75575	1.32319	0.00710	0.60765	...
3	0.61750	1.61942	0.00506	0.93472	...
4	0.53824	1.85790	0.00229	0.42326	...
5	1.33086	0.75139	0.00244	0.73243	$f_1 + f_2$
6	0.14193	7.04554	0.00283	0.17699	...
7	1.15390	0.86662	0.00183	0.40790	$3f_{11} - 2f_6$
8	0.84792	1.17936	0.00173	0.21712	...
9	0.17696	5.65111	0.00175	0.03446	$f_5 - f_7$
10	1.19445	0.83720	0.00181	0.26549	$3f_7 - 3f_2$
11	0.47926	2.08657	0.00221	0.93443	$2f_3 - f_2$
12	0.72073	1.38749	0.00154	0.68085	...
13	0.34838	2.87041	0.00164	0.42315	...
14	0.50875	1.96560	0.00160	0.19069	...
Sector 48					
1	0.57216	1.74775	0.00525	0.38656	...
2	0.75754	1.32007	0.00550	0.85755	...
3	0.62029	1.61215	0.00363	0.43581	...
4	0.51691	1.93458	0.00268	0.54496	...
5	0.03208	31.16825	0.00215	0.21009	...
6	0.47413	2.10913	0.00230	0.77090	...
7	0.13368	7.48038	0.00208	0.60656	...
8	1.20136	0.83239	0.00152	0.39080	...
9	0.54721	1.82745	0.00206	0.45903	$2f_6 - 3f_7$
10	1.16750	0.85653	0.00128	0.24873	$f_3 + f_9$
11	1.06946	0.93505	0.00130	0.63961	$3f_9 - f_1$
12	1.24058	0.80608	0.00121	0.14613	$2f_1 + 3f_5$
13	0.65416	1.52869	0.00111	0.73331	$f_8 - f_9$
14	0.32797	3.04907	0.00130	0.31276	$2f_6 - 1f_3$
15	1.46338	0.68335	0.00114	0.02072	...
16	0.79853	1.25230	0.00105	0.94676	...
17	1.33327	0.75004	0.00105	0.18225	$2f_2 - 2f_{18}$
18	0.09090	11.00056	0.00115	0.97135	$3f_9 - 3f_4$
19	0.27628	3.61954	0.00136	0.20454	$2f_4 - f_2$
Sector 49					
1	0.58305	1.71511	0.00559	0.83908	...
2	0.62404	1.60247	0.00431	0.54603	$f_{13} + 3f_{orb}$
3	0.72463	1.38002	0.00290	0.52369	...
4	1.20709	0.82844	0.00154	0.65613	$f_1 + f_2$
5	0.69296	1.44309	0.00146	0.80110	$f_4 - 3f_6$
6	0.17138	5.83509	0.00153	0.62546	...
7	0.11363	8.80046	0.00138	0.03058	...
8	0.77306	1.29356	0.00127	0.24628	...
9	0.50854	1.96640	0.00101	0.29600	$f_1 - 2f_{12}$
10	1.08042	0.92557	0.00100	0.44376	$f_4 + 2f_{orb}$
11	1.33004	0.75186	0.00119	0.77884	...
12	0.03726	26.84140	0.00120	0.14437	...
13	0.43962	2.27469	0.00102	0.26426	$f_2 - 3f_{orb}$
14	1.45857	0.68560	0.00083	0.19028	...
15	1.28905	0.77576	0.00084	0.71994	$3f_2 - f_1$
16	0.30364	3.29342	0.00095	0.51397	$3f_7 - f_{12}$
17	0.90159	1.10915	0.00082	0.90908	$3f_9 - f_2$
18	1.49396	0.66936	0.00077	0.86441	$f_1 + 3f_{16}$
Sector 50					
1	0.58505	1.70925	0.00713	0.08703	...
2	0.75656	1.32176	0.00538	0.50804	...
3	0.63269	1.58054	0.00299	0.64490	...
4	0.14102	7.09108	0.00300	0.95761	...
5	0.70892	1.41059	0.00233	0.55521	...
6	1.33590	0.74856	0.00181	0.99306	...
7	1.45596	0.68683	0.00145	0.46174	$2f_3 + f_{10}$
8	0.03621	27.61790	0.00150	0.50930	...
9	1.29779	0.77054	0.00148	0.08374	...
10	0.19057	5.24740	0.00147	0.02102	$f_5 - f_{11}$
11	0.51835	1.92919	0.00174	0.61283	...

(*continued on next page*)

Table A.5 (*continued*).

No	Frequency (d^{-1})	Period (days)	Amplitude (mag)	Phase (rad)	Combination
12	0.46499	2.15057	0.00136	0.39848	$2f_{11} - 3f_{10}$
13	1.51504	0.66005	0.00121	0.84776	$f_1 + 2f_{12}$
14	1.37592	0.72679	0.00095	0.49814	...
15	2.04482	0.48904	0.00094	0.97961	$f_5 + f_6$
16	0.67653	1.47814	0.00096	0.40019	...
Sector 53					
1	0.58243	1.71694	0.00649	0.62019	...
2	0.71253	1.40345	0.00475	0.41628	...
3	0.12609	7.93063	0.00259	0.92785	...
4	0.76857	1.30112	0.00262	0.44097	...
5	0.61245	1.63278	0.00212	0.93945	...
6	1.30096	0.76866	0.00198	0.71286	...
7	0.36427	2.74522	0.00158	0.58762	$f_6 - 2f_9$
8	0.02802	35.68783	0.00140	0.16284	...
9	0.46835	2.13517	0.00160	0.67008	$3f_4 - 3f_5$
10	0.42031	2.37919	0.00148	0.41751	...
11	0.99674	1.00327	0.00106	0.78124	$3f_5 - 2f_{10}$
12	1.03477	0.96640	0.00097	0.09625	$3f_1 - f_2$
13	0.95471	1.04744	0.00096	0.74557	$2f_4 - f_1$
14	0.50437	1.98266	0.00101	0.72681	$3f_8 + f_{10}$
Sector 56					
1	0.57746	1.73173	0.01045	0.80446	...
2	0.76038	1.31513	0.00409	0.40135	...
3	0.13629	7.33707	0.00347	0.58460	...
4	0.45013	2.22158	0.00215	0.24699	...
5	0.71913	1.39057	0.00216	0.68785	...
6	1.15133	0.86856	0.00210	0.49736	...
7	0.18471	5.41376	0.00157	0.11016	$3f_{orb}$
8	1.29121	0.77447	0.00153	0.94883	$2f_1 + f_3$
9	0.49138	2.03510	0.00162	0.62370	$2f_4 - 3f_3$
10	0.02869	34.85107	0.00121	0.04972	...
11	0.07353	13.60042	0.00132	0.32705	...
12	0.89667	1.11523	0.00114	0.34843	$f_2 + f_3$
13	0.35150	2.84499	0.00107	0.16930	$f_2 - 3f_3$

References

Ammons, S.M., Robinson, S.E., Strader, J., Laughlin, G., Fischer, D., Wolf, A., 2006. Astrophys. J. 638, 1004A.

Bai, Y., Liu, J.F., Bai, Z.R., Wang, S., Fan, D.W., 2019. Astron. J. 158, 93.

Cannon, A.J., Pickering, E.C., 1993. Henry Draper Catalogue and Extension. 1993yCat.3135....0C1993/10.

Chen, Y., Bressan, A., Girardi, L., Marigo, P., Kong, X., Lanza, A., 2015. Mon. Not. R. Astron. Soc. 452, 1068.

Cox, A.N., 1999. Allen's Astrophysical Quantities, fourth ed.

Davies, D., 2015. Peremenn. Zvezdy Prilozheine 15, 1, 2015PZP....15....1D.

Debosscher, J., Aerts, C., Tkachenko, A., et al., 2013. Astron. Astrophys. 556, A56.

Eker, Z., Bakış, V., 2023. Mon. Not. R. Astron. Soc. 523, 2440.

Eker, Z., Soyduğan, F., Bilir, S., et al., 2020. Mon. Not. R. Astron. Soc. 496, 3887.

Gaia Collaboration, 2018. Astron. Astrophys. 616A.

Gaia Collaboration, 2020. 2020yCat.1350....0G.

Gaia Collaboration, 2022. 2022yCat.1355....0G.

Gebran, M., Paletou, F., Bentley, I., et al., 2023. Deep learning applications for stellar parameter determination: II-application to the observed spectra of AFGK stars. Open Astron. 32, 1, 2023OAst...32..209G.

Girardi, L., Bressan, A., Bertelli, G., Chiosi, C., 2000. Astron. Astrophys. 141, 371.

Gray, R.O., Corbally, C.J., Burgasser, A.J., et al., 2008. Stellar Spectral Classification. Princeton University Press, ISBN: 978-0-691-12510-7.

Grigahcène, A., Antoci, V., Balona, L., et al., 2010. Astrophys. J. 713, L192.

Gürol, B., 2023. New Astron. 103, 102052.

Henry, G.W., Fekel, F.C., Henry, S.M., 2005. Astron. J. 129, 2815.

Jayasinghe, T., Stanek, K.Z., Kochanek, C.S., et al., 2019. Mon. Not. R. Astron. Soc. 486, 1907.

Kaye, A.B., Handler, G., Krisciunas, K., et al., 1999. Publ. Astron. Soc. Pac. 111, 840.

Kim, C.H., Kreiner, J.M., Zakrzewski, B., Ogloza, W., Kim, H.W., Jeong, M.J., 2018. Astrophys. J. Suppl. 235, 41.

Kopal, Z., 1978. ASSL (Astrophysics and Space Science Library), Vol. 68. D. Reidel Publishing Co., Dordrecht.

Kurtz, D.W., Shibahashi, H., Murphy, S.J., Bedding, T.R., Bowman, D.M., 2015. Mon. Not. R. Astron. Soc. 450, 3015.

Lenz, P., Breger, M., 2005. Commun. Asteroseismol. 146, 53.

Li, G., Guo, Z., Fuller, J., et al., 2020. Mon. Not. R. Astron. Soc. 497, 4363.

Maceroni, C., Lehmann, H., da Silva, R., Montalbán, J., 2015. EPJ Web Conf. 101, 04003.

Maceroni, C., Lehmann, H., da Silva, R., et al., 2014. Astron. Astrophys. 563, A59.

Maceroni, C., Montalbán, J., Gandolfi, D., Pavlovski, K., Rainer, M., 2013. Astron. Astrophys. 552, A60.

McDonald, I., Zijlstra, A.A., Watson, R.A., 2017. Mon. Not. R. Astron. Soc. 471, 770.

Paunzen, E., Bernhard, K., Hümmerich, S., et al., 2020. Mon. Not. R. Astron. Soc. 499, 3976.

Prša, A., Kochoska, A., Conroy, K.E., et al., 2022. TESS eclipsing binary stars. I. Short-cadence observations of 4584 eclipsing binaries in sectors 1-26. Astrophys. J. Suppl. 258, 1.

Ricker, G.R., Winn, J.N., Vanderspek, R., et al., 2015. Transiting exoplanet survey satellite (TESS). J. Astron. Telesc. Instr. Syst. 1, 014003. http://dx.doi.org/10.1117/1.JATIS.1.1.014003.

Stassun, K.G., Oelkers, R.J., Paegert, M., et al., 2019. The revised TESS input catalog and candidate target list. Astron. J. 158, 138.

Stevens, D.J., Stassun, K.G., Gaudi, B.S., 2017. Astron. J. 154, 259.

Straizys, V., Kurilliene, G., 1981. Astrophys. Space Sci. 80, 353.

Tonry, J.L., Denneau, L., Flewelling, H., et al., 2018. Astrophys. J. 867, 105.

Warner, P.B., Kaye, A.B., Guzik, J.A., 2003. Astrophys. J. 593, 1049.

Wilson, R.E., 1979. Astrophys. J. 234, 1054.

Wilson, R.E., 1990. Astrophys. J. 256, 613.

Wilson, R.E., Devinney, E.J., 1971. Astrophys. J. 166, 605.

Wilson, R.E., van Hamme, W., 2007. Documentation of Eclipsing Binary Compute Model. Astronomy Department, University of Florida, Gainesville.

Wright, C.O., Egan, M.P., Kraemer, K.E., Price, S.D., 2003. Astron. J. 125, 259.

Zhang, X.B., Chen, X.H., Zhang, H., Fu, J., Li, Y., 2020. Astrophys. J. 895, 124.

Zhang, X.B., Wang, K., Chen, X.H., Luo, C.Q., Zhang, C.G., 2019. Astrophys. J. 884, 165.

Zombeck, M.V., 2004. Handbook of Space Astronomy & Astrophysics, second ed. Cambridge University Press.